Raman electron paramagnetic resonance in $Zn_{1-x}Cr_xTe$ and $Cd_{1-x}Cr_xTe$

X. Lu, S. Tsoi, I. Miotkowski, S. Rodriguez, and A. K. Ramdas
Department of Physics, Purdue University, West Lafayette, Indiana 47907, USA

H. Alawadhi
Department of Basic Sciences, University of Sharjah, Sharjah, United Arab Emirates

(Received 21 November 2006; published 25 April 2007)

Raman electron paramagnetic resonance (Raman-EPR) of the transitions due to the spin flip of the $3d$ electrons of Cr^+ in $Zn_{1-x}Cr_xTe$ and $Cd_{1-x}Cr_xTe$ is observed at $\hbar\omega_{PM}=g(Cr^+)\mu_B B$ with $g(Cr^+)=2.0041\pm0.0095$ and 2.0039 ± 0.0093, respectively. The appearance of Raman lines at $\omega_{LO}\pm n\omega_{PM}$, $n=1$, 2, and 3 results from the strong Fröhlich interaction with the zone-center longitudinal-optic phonon. The intensity of the Raman-EPR of Cr^+ can be enhanced through the photogeneration process by simultaneous illumination with photons having an energy close to the excitonic band gap; photoluminescence spectra reveal signatures of excitons bound to Cr^+ acceptors in $Zn_{1-x}Cr_xTe$ specimens. The resonance profile of Cr^+ Raman-EPR shows that the strong resonant enhancement is mediated via an exciton bound to a neutral acceptor.

DOI: 10.1103/PhysRevB.75.155206 PACS number(s): 78.30.−j, 78.20.Ls, 78.55.Et

I. INTRODUCTION

The electronic structure of a free chromium atom is $3d^54s^1$ rather than $3d^44s^2$, the half-filled $3d$ shell being a more stable configuration. As a constituent of a II-VI ternary, chromium replaces the cations substitutionally, resulting in a Cr-based diluted magnetic semiconductor (DMS),[1] e.g., $Zn_{1-x}Cr_xTe$ or $Cd_{1-x}Cr_xTe$. This substitutional incorporation with the completion of the tetrahedral bonding can occur in several ways: (1) The electronic configuration of Cr can be "$3d^44s^2$," with the two $4s$ electrons incorporated in the tetrahedral bonding scheme, resulting in Cr^{2+} as an isoelectronic center (X^0). (2) In a second scenario, an electron is "borrowed" from the valence band of the host, resulting in the "$3d^54s^2$" configuration; in this case, only one $4s$ electron of Cr is incorporated in the tetrahedral bonding scheme, making it Cr^+ and causing the other electron 'borrowed' from the valence band to result in a negatively charged center (X^-) to which the hole is bound. (3) Chromium can also be in Cr^{3+} state in which one $4s$ and one $3d$ electron are incorporated in the bonding scheme, while another $3d$ electron is donated to the conduction band, leaving the Cr center positively charged (X^+); the X^+ center can bind the free electron, making Cr a single donor. The electronic configuration of the Cr^{3+} ion is $3d^3$. The energy-level structure of the chromium ion, which when incorporated substitutionally replaces the cation of a zinc-blende II-VI host and hence has T_d site symmetry, followed by a crystal field, a spin-orbit interaction, and a Jahn-Teller distortion (when appropriate), is discussed in Sec. III B.

Cr-based DMSs share with the other DMSs remarkable magnetic and magneto-optic properties, originating in the so-called "*sp-d*" exchange interaction between the band carriers and localized $3d$ electrons. The most striking difference between Cr-based DMSs, on the one hand, and the Mn-, Co-, and Fe-based DMSs, on the other, is the ferromagnetic *p-d* exchange interaction between valence-band electrons and Cr ions in the former, and the antiferromagnetic interaction in the latter. The ferromagnetic character of *p-d* exchange interaction in Cr-based DMSs has been investigated theoretically[2,3] and manifested through magneto-reflectance measurements[4–7] in $Zn_{1-x}Cr_xSe$, $Zn_{1-x}Cr_xS$, $Zn_{1-x}Cr_xTe$, and $Cd_{1-x}Cr_xS$. The ferromagnetic *sp-d* exchange interaction may also mediate the ferromagnetic coupling between Cr ions. Recently, magnetic circular dichroism in $Zn_{1-x}Cr_xTe$ films (with $x=0.2$) has revealed the occurrence of room-temperature (300 K) ferromagnetism.[8,9] Saito *et al.*[8] claimed that $Zn_{1-x}Cr_xTe$ is the third real ferromagnetic DMS after $In_{1-x}Mn_xAs$ and $Ga_{1-x}Mn_xAs$, in which the *sp-d* exchange interaction could be used to develop spintronic[10] devices. Pekarek *et al.*[11] showed that even in bulk $Zn_{1-x}Cr_xTe$ with small x ($x=0.0033$), due to the low solubility of Cr in ZnTe and thus the inhomogeneity of the crystal, the magnetization in a Cr rich region exhibits ferromagnetism with a transition temperature well above room temperature, viz., 365 K.

The Cr^{2+} state in Cr-doped II-VI DMSs has been observed in electron paramagnetic rosonance (EPR)[12,13] and optical absorption,[14] as well as in magnetization and specific heat measurements.[4,15–18] It was discovered that by illuminating the specimens containing Cr^{2+} with photons of an appropriate energy, Cr^+ can be photogenerated. EPR and photo-EPR studies of Cr^+ state in Cr-doped II-VI DMSs have been reported in ZnS,[19–24] ZnSe,[24–26] ZnTe,[24–26] and CdTe.[27] Cr^{3+} state has also been reported to exist in Cr-doped ZnSe.[28]

The microscopic mechanism for the unique magnetic properties and the astonishing *p-d* exchange character of Cr-based DMSs is yet to be identified. EPR or Raman-EPR can provide important insights into the electronic configuration of the $3d$ transition metal ion (TMI) in the DMS alloy directly responsible for the magnetization and magnetic properties of the material investigated. We report and discuss our results on the Raman-EPR of Cr^+ in ZnTe and CdTe in this context.

II. EXPERIMENT

$Zn_{1-x}Cr_xTe$ and $Cd_{1-x}Cr_xTe$ crystals were grown using the modified vertical Bridgman method with nominal Cr concen-

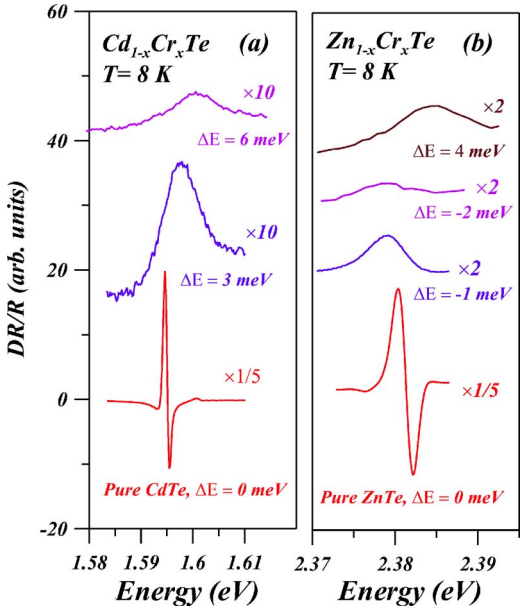

FIG. 1. (Color online) Wavelength modulated reflectivity spectra of (a) $Cd_{1-x}Cr_xTe$ and (b) $Zn_{1-x}Cr_xTe$ at 8 K displaying the free excitonic signatures. The spectra are shifted vertically for clarity.

trations limited to $\leqslant 2\%$ due to Cr's low solubility. The technique for obtaining wavelength modulated reflectivity (WMR) is discussed in detail in Ref. 29. Photoluminescence (PL) and Raman spectra were recorded with a double-grating monochromator (and a third grating operating in tandem for a more rigorous rejection of parasitic radiation when necessary) and a photon-counting detector incorporating a cooled photomultiplier. A Janis superconducting optical cryostat was employed in the application of magnetic fields up to 6 T and to achieve temperatures as low as 1.8 K. Measurements were performed on oriented $(1\bar{1}0)$ cleaved surfaces, allowing a magnetic field to be applied along [001], [110], and [111]. The samples were excited with a 5208 Å line from a Kr^+ laser, a 5145 Å line from an Ar^+ laser, a Coherent 599 Dye laser (with coumarin 7 dye), or with a Coherent CR 899 tunable Ti:sapphire laser.

III. RESULTS AND DISCUSSION

A. Characteristics of the excitonic band gap

WMR spectra of $Cd_{1-x}Cr_xTe$ and $Zn_{1-x}Cr_xTe$ for several nominal values of x are shown in Figs. 1(a) and 1(b), respectively. The excitonic band gaps (E_g) deduced from the peak fits for the signatures in WMR spectra for $Zn_{1-x}Cr_xTe$ show distinct shifts (ΔE) from that for pure ZnTe, from −2 to 4 meV; the ΔE's for the two $Cd_{1-x}Cr_xTe$ specimens are 3 and 6 meV. Even in the absence of a precise knowledge of x and of its departure from the nominal value for the specimens investigated, we can conclude that (i) ternary alloys of $Zn_{1-x}Cr_xTe$ and $Cd_{1-x}Cr_xTe$ have formed and (ii) the excitonic band gap $[E_g(x)]$ of $Cd_{1-x}Cr_xTe$ shifts to values higher than that of pure CdTe; the negative shifts of $E_g(x)$ in the two $Zn_{1-x}Cr_xTe$ specimens below that of pure ZnTe may be an indication of bowing as in $ZnSe_xTe_{1-x}$ (Ref. 30). It appears that for a definitive statement about the x dependence of $E_g(x)$ in $Cd_{1-x}Cr_xTe$ and $Zn_{1-x}Cr_xTe$, one has to resort to nonequilibrium growth techniques, such as molecular beam epitaxy (MBE) or metal-organic chemical-vapor deposition (MOCVD). Indeed, Mak *et al.*[31] have reported a significantly larger range of x in MBE grown $Zn_{1-x}Fe_xSe$.

B. Electronic energy structure of Cr in ZnTe and CdTe

Villeret *et al.*[32] have systematically investigated the low-lying levels and Zeeman splittings of TMIs (with the $3d^n$ electronic configuration, $n=1-9$) in DMSs having the zinc-blende or the wurtzite structure. The electronic energy structure of Cr^{2+} including the Jahn-Teller effect has been reported in several papers,[13,14] for example, in Fig. 10 of Ref. 13. The ground state of a Cr^{2+} free ion is ${}^5D(L=2,S=2)$ with an orbital and spin quintet. The crystal field with T_d symmetry splits ${}^5D$ into an orbital triplet ${}^5\Gamma_5$ and an orbital doublet ${}^5\Gamma_3$. The ${}^5\Gamma_5$ state is very sensitive to a static tetragonal Jahn-Teller distortion, which leads to further splitting of the ground state into an orbital doublet ${}^5\Gamma_5$ and an orbital singlet ${}^5\Gamma_4$. The spin-orbit coupling results in still further splittings. The ${}^5\Gamma_4$ state breaks up into a singlet Γ_4, a doublet Γ_5, and two unresolved singlets Γ_1 and Γ_2. For Cr in ZnTe and CdTe, due to a strong covalency effect,[14,33] the singlet Γ_4 is the ground state, followed by Γ_5, and Γ_1,Γ_2. Since the ground state of Cr^{2+} in ZnTe and CdTe is a singlet, but with excited states close enough to contribute to magnetic properties, the magnetization of Cr^{2+} exhibits a paramagnetism intermediate between those of the van Vleck and Brillouin cases. The magnetization measurements by Pekarek *et al.*[17,18] showed that majority of Cr ions in ZnTe and CdTe are in the Cr^{2+} state.

The ground state of Cr^+ is ${}^6S_{5/2}$ $(S=5/2,L=0)$ with a sixfold spin degeneracy. Under the crystal field of T_d symmetry, the ground state splits into a Γ_8 quadruplet and a Γ_7 doublet with a very small splitting.[34] With spin-orbit interaction absent (since $L=0$), the ground state of Cr^+, similar to that of Mn^{2+}, can be treated as an atomic ${}^6S_{5/2}$ level. The magnetization of Cr^+ should display a paramagnetism which follows a $B_{5/2}$ Brillouin function just as Mn-based DMSs do.

Cr^{3+} ion has the same electronic configuration as V^{2+} and thus the two have a similar electronic energy structure as well. The ground state ${}^4F$ $(L=3,S=3/2)$ (see Ref. 35) in a tetrahedral crystal field with T_d site symmetry is an orbital triplet ${}^4\Gamma_4$ (Ref. 32), which results in an orbital singlet ${}^4\Gamma_2$ with a fourfold spin degeneracy[36] when a Jahn-Teller distortion is combined with spin-orbital coupling. Cr^{3+} thus displays a paramagnetism which follows a $B_{3/2}$ Brillouin function, as shown by Tsoi *et al.*[39] for V^{2+} in CdTe.

C. Magnetic-field-induced Raman excitations in $Zn_{1-x}Cr_xTe$ and $Cd_{1-x}Cr_xTe$

Figure 2 shows the Raman spectrum of $Zn_{1-x}Cr_xTe$ recorded at 8 K in an external magnetic field of 6 T parallel to [001]. The Raman shift labeled "PM" and its multiples up to the fourth order are clearly observed in the Stokes, and up to

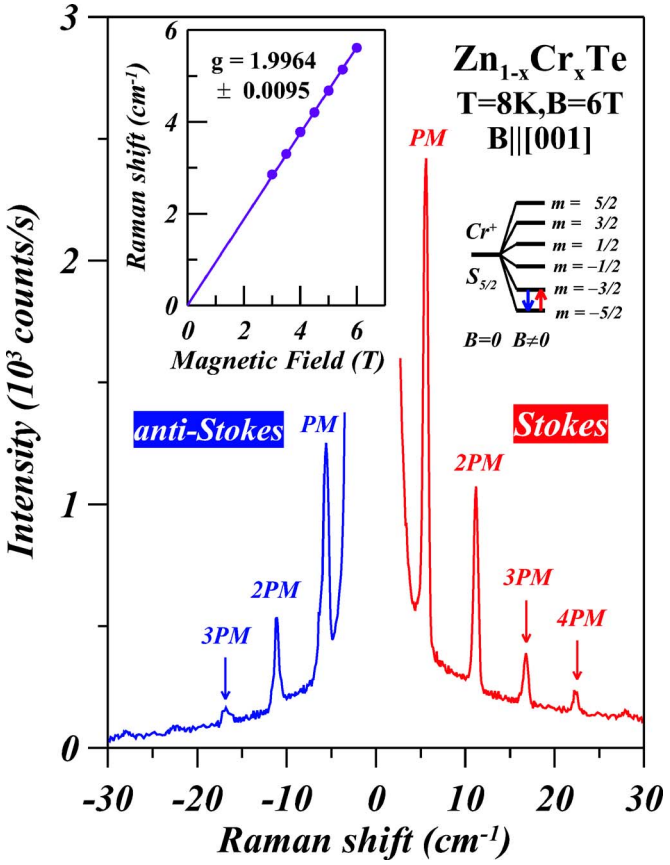

FIG. 2. (Color online) The Stokes Raman line labeled "PM" and its multiples up to the fourth order, as well as the anti-Stokes Raman line up to the third order measured in $Zn_{1-x}Cr_xTe$. The excitation energy is $\hbar\omega_L$=2.3481 eV (from a Coherent 599 dye laser with coumarin 7 dye) with incident power ~150 mW, and the spectrum was recorded at 8 K and 6 T.

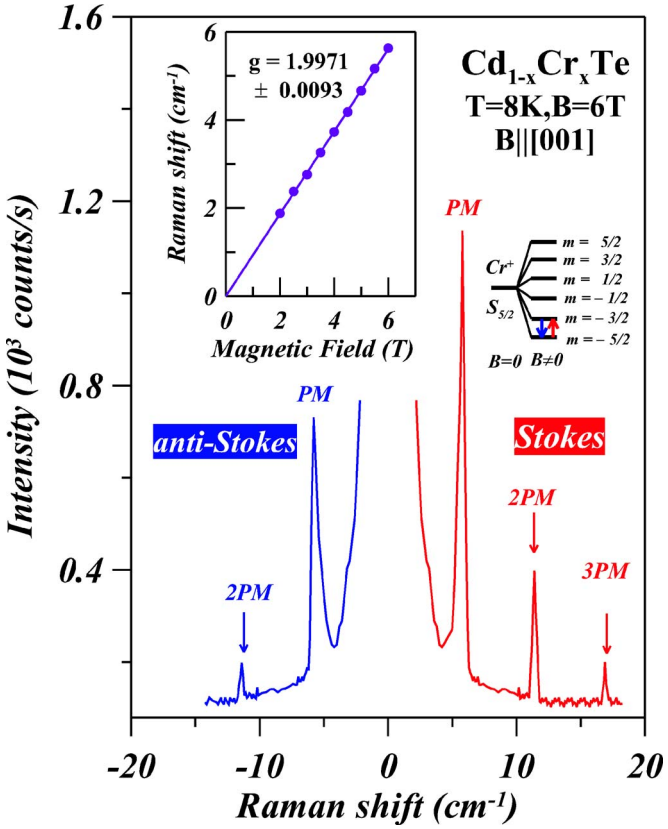

FIG. 3. (Color online) The Stokes Raman line labeled "PM" and its multiples up to the third order, as well as the anti-Stokes Raman line up to the second order measured in $Cd_{1-x}Cr_xTe$. The excitation energy is $\hbar\omega_L$=1.5885 eV from the Coherent CR899 tunable Ti-:sapphire laser with incident power ~150 mW, and the spectrum was recorded at 8 K and 6 T.

the third order in the anti-Stokes, spectrum. The Raman shift for PM as a function of applied field up to 6 T, shown in the inset, is linear in B and yields g=1.9964. The values of g for $\mathbf{B}\|[110]$ and [111] are 2.0023 and 2.0130, respectively. We thus conclude that, within experimental errors, the Raman shift of the PM feature in $Zn_{1-x}Cr_xTe$ is isotropic with an average g=2.0041±0.0095. The results for $Cd_{1-x}Cr_xTe$ are shown in Fig. 3 for $\mathbf{B}\|[001]$. The linearity of the Raman shift as a function of B yields g factors of 1.9971, 2.0092, and 2.0054 for **B** along [001], [110], and [111], respectively. Based on this isotropy within experimental errors in $Cd_{1-x}Cr_xTe$, an average g=2.0039±0.0093 is deduced.

Magnetization measurements by Pekarek *et al.*[17,18] show that a large majority of Cr ions in $Zn_{1-x}Cr_xTe$ and $Cd_{1-x}Cr_xTe$ are in the Cr^{2+} charge state. Thus, one expects to see the electronic transitions between the low-lying energy levels of Cr^{2+} [a singlet Γ_4 with m_s=0, a doublet Γ_5 with m_s=±1 occurring 2.3 cm^{-1} above Γ_4 at B=0 (Ref. 13), and the two unresolved Γ_1, Γ_2 singlets with m_s=±2] and their Zeeman sublevels in the presence of magnetic field. In addition, due to a strong Jahn-Teller effect, the EPR of Cr^{2+} in ZnTe and CdTe (Refs. 12 and 13) shows anisotropic features, most of them being nonlinear with respect to B. The EPR of Cr^{3+} is expected to be similar to that of V^{2+} [e.g., V^{2+} in CdTe (Ref. 36) and ZnTe (Ref. 37)], which exhibits an anisotropic g factor as a result of the Jahn-Teller distortion; in addition, theoretical calculations by Oshiyama *et al.*[38] predict the g factor of Cr^{3+} to be ~1.95. We therefore rule out Cr^{2+} and Cr^{3+} as being responsible for the isotropic Raman feature PM discussed above and for its linear shifts with B. In contrast, Cr^+, with its ground state identical to that of $Mn^{2+}(^6S_{5/2})$, should exhibit a ground-state Zeeman multiplet given by $E(m_s)=g\mu_B Bm_S$; here, the projection of **S** along **B**, m_S, is −5/2, −3/2, −1/2, 1/2, 3/2, or 5/2. One can thus attribute the isotropic PM line to $\Delta m_S=\pm 1$ and consider its linear shifts as a function of B to Cr^+ in ZnTe and CdTe, arising from the electron spin-flip transitions between adjacent sublevels of the Zeeman multiplet of Cr^+ in $Zn_{1-x}Cr_xTe$ and $Cd_{1-x}Cr_xTe$. Following Refs. 40 and 41, we label them as Raman electron paramagnetic resonance (Raman-EPR). Within experimental errors, the g factors of Cr^+ in ZnTe and CdTe deduced from our Raman-EPR measurements show excellent agreement with those measured from EPR, viz., 2.0023±0.0005 in ZnTe (Ref. 25) and 1.9997±0.0003 in CdTe (Ref. 27), and with the theoretically calculated value of 1.999 in ZnS.[38] We note that the g factors of Cr^+ and Mn^{2+}, say, in CdTe, are ~2, due to the negligible mixing of the ground state with higher-lying orbital states (in $Cd_{1-x}Mn_xTe$, the next level is about 2.4 eV higher than the ground level).

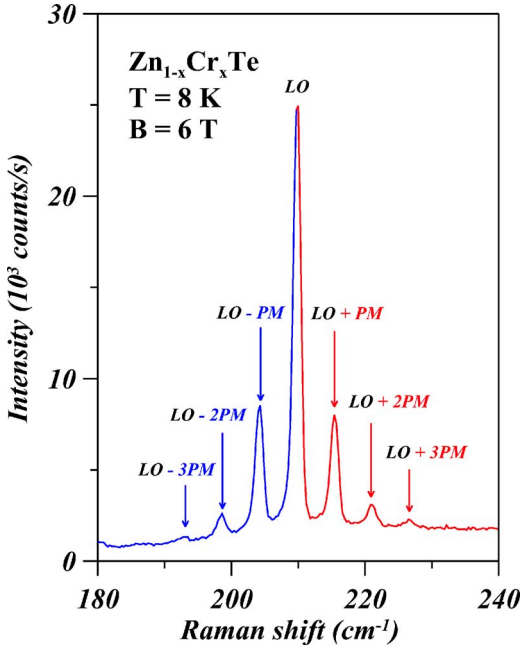

FIG. 4. (Color online) Raman spectrum showing LO phonon in $Zn_{1-x}Cr_xTe$ and its satellites at frequency shifts $\omega_{LO}\pm\omega_{PM}$, $\omega_{LO}\pm2\omega_{PM}$, and $\omega_{LO}\pm3\omega_{PM}$. The excitation energy is $\hbar\omega_L$ =2.3798 eV (5208 Å line from a Kr^+ laser) with incident power ~150 mW, and the spectrum was recorded at 8 K and 6 T.

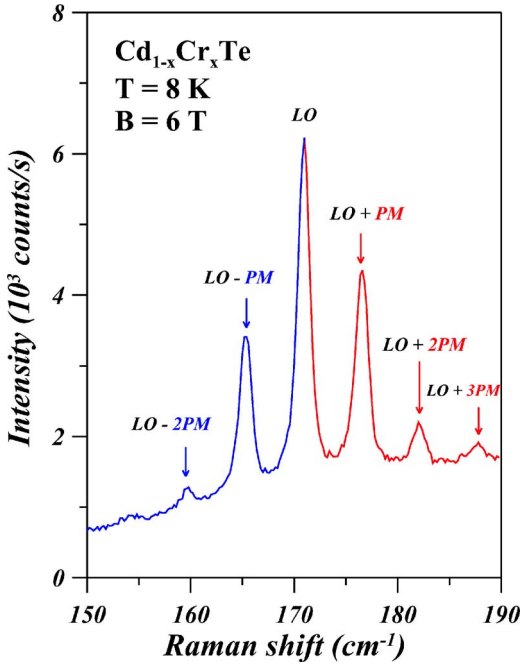

FIG. 5. (Color online) Raman spectrum showing the combination of LO phonon in $Cd_{1-x}Cr_xTe$ and its satellites at frequency shifts $\omega_{LO}\pm\omega_{PM}$, $\omega_{LO}\pm2\omega_{PM}$, and $\omega_{LO}\pm3\omega_{PM}$. The excitation energy is $\hbar\omega_L$=1.5885 eV from the Coherent CR899 tunable Ti:sapphire laser with incident power ~150 mW, and the spectrum was recorded at 8 K and 6 T.

The nearly identical g values of Cr^+ in ZnTe and CdTe show that the small difference in covalent bonding observed in microwave EPR measurements of Title[25] is not noticeable in Raman-EPR due to the larger experimental error in the latter.

Figures 4 and 5 show the Raman spectrum of the zone-center LO phonon[54] with satellites at $\omega_{LO}\pm\omega_{PM}$, $\omega_{LO}\pm2\omega_{PM}$, and $\omega_{LO}\pm3\omega_{PM}$ in $Zn_{1-x}Cr_xTe$ and $Cd_{1-x}Cr_xTe$, respectively. In the [110] backscattering geometry employed in the experiment, the LO phonon is forbidden in all polarization configurations (see Ref. 42); its appearance with a large intensity in the forbidden geometry for a zinc-blende crystal has been ascribed to the resonance enhancement coupled with the Fröhlich interaction,[43] as has been noted by Limmer *et al.*[44] The microscopic process resulting in $\omega_{LO}+\omega_{PM}$ involves the creation of an LO phonon and the excitation of a Cr^+ to the next higher sublevel of the Zeeman multiplet of the ground state, and the shift of $\omega_{LO}-\omega_{PM}$ involves the creation of an LO phonon and the deexcitation of a Cr^+ to the next lower sublevel of the Zeeman multiplet.

The absence of the internal transitions of Cr^{2+} in our Raman measurements on ZnTe and CdTe could be due to the strong intensity of the Raman-EPR of Cr^+ under resonance conditions overriding the weak internal transitions of Cr^{2+}, e.g., the 2.3 cm^{-1} $\Gamma_4\rightarrow\Gamma_5$ transition.[13] In addition, in Raman-EPR, with the incident light having an energy close to the band gap to achieve resonance enhancement, the Cr^{2+} appears to experience photoconversion into Cr^+.

Figure 6 shows the intensity of the Raman-EPR of Cr^+ in ZnTe when subjected to a simultaneous illumination with radiation having an energy close to the band gap, recorded at 8 K and 6 T. In Fig. 6(a), the incident radiation power I_1

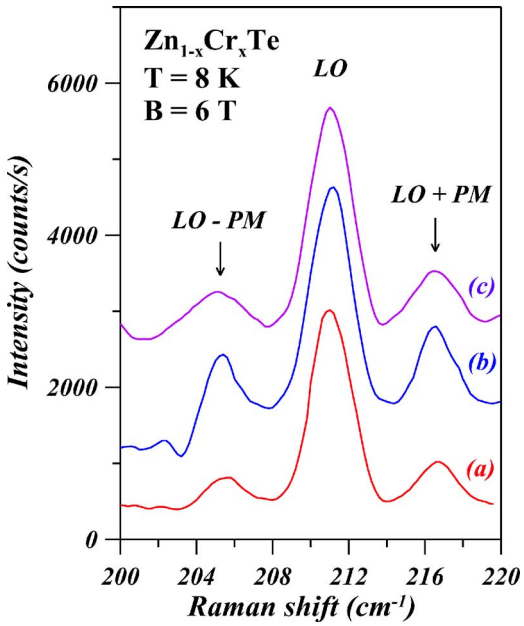

FIG. 6. (Color online) Comparison of the Cr^+ Raman-EPR intensities in ZnTe in the presence of simultaneous illumination of radiation with an energy close to the band gap, recorded at 8 K and 6 T. The incident radiation (I_1) is the Kr^+ 5208 Å line; the simultaneous illumination radiation (I_2) is the Ar^+ 5145 Å line. (a) I_1 =10 mW, I_2=0; (b) I_1=10 mW, I_2=100 mW; (c) I_1=10 mW, I_2 =200 mW.

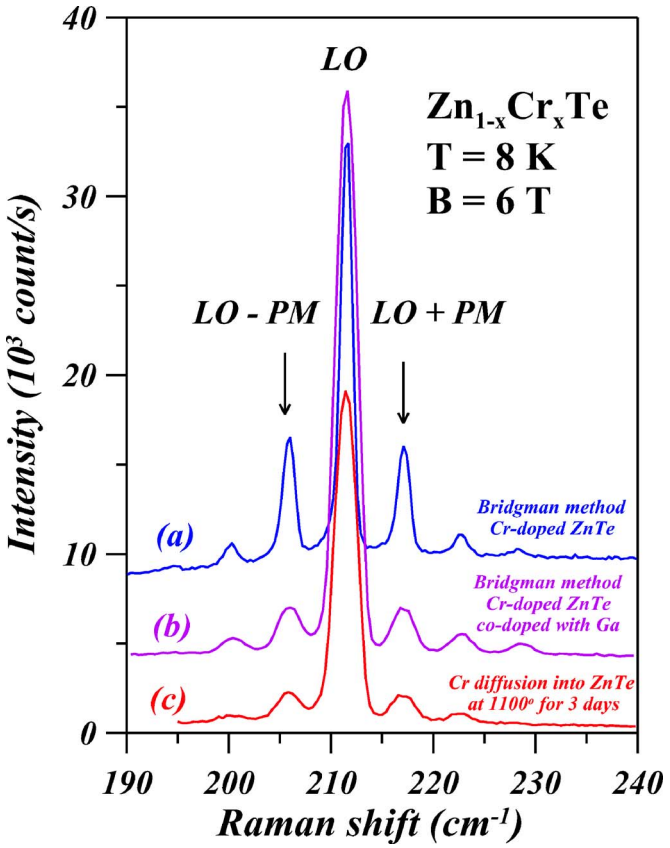

FIG. 7. (Color online) Comparison of the Cr^+ Raman-EPR intensities in ZnTe at LO±PM, recorded at 8 K and 6 T, for three different crystal growth methods: (a) Bridgman method, Cr-doped ZnTe; (b) Bridgman method, Cr-doped and Ga-codoped ZnTe; and (c) Cr diffusion into ZnTe at 1100 °C for 3 days.

=10 mW of the Kr^+ line at 5208 Å, and the Raman spectrum shows signatures of the LO phonon, accompanied by the Stokes and anti-Stokes Raman lines at $\omega_{LO}\pm\omega_{PM}$. In Fig. 6(b), the 5145 Å line from an Ar^+ laser with I_2=100 mW illuminates the same spot on the sample as that of the incident radiation. As can be seen, the intensity at $\omega_{LO}\pm\omega_{PM}$ increases by a factor of 2, while that at ω_{LO} remains unchanged. Thus, the increased intensity of $\omega_{LO}\pm\omega_{PM}$ in Fig. 6(b) can be attributed to an increase in the Cr^+ concentration in ZnTe as a result of the simultaneous illumination with the 5145 Å line, as a result of the conversion of Cr^{2+} to Cr^+ by photoconversion. The underlying microscopic mechanism is as follows: the 5145 Å photon creates an electron-hole pair, an electron in the conduction band and a hole in the valence band; the electron in the conduction band then binds to Cr^{2+}, generating Cr^+ as an acceptor center. An increase in I_2 beyond 200 mW broadens $\omega_{LO}\pm\omega_{PM}$ without changing the integrated intensity, as can be seen in Fig. 6(c). A similar experiment to observe the photoconversion of Cr^{2+} into Cr^+ in CdTe was not successful.

Another possible way of increasing the Cr^+ concentration is by the introduction of the trivalent ions (e.g., Ga^{3+}), as suggested by Vallin *et al.*[14] Figure 7 shows the intensity comparison of Raman lines at $\omega_{LO}\pm\omega_{PM}$ with different crystal growth methods: (a) Bridgman method, Cr-doped ZnTe; (b) Bridgman method, Cr-doped and Ga-codoped ZnTe; (c) Cr diffusion into ZnTe at 1100 °C for 3 days. The intensities of LO features in all three cases are comparable, indicating good and similar crystal quality. The intensity at $\omega_{LO}\pm\omega_{PM}$ Raman lines in Fig. 7(a) is much stronger than that in Fig. 7(b), demonstrating that codoping with Ga has not effectively increased but may have somewhat decreased the concentration of the Cr^+ acceptor centers. In other words, the photoconversion process $Cr^{2+}\rightarrow Cr^+$ is a more effective way to produce Cr^+ centers. Diffusion of Cr into ZnTe at high temperature can also incorporate enough Cr in ZnTe to observe Cr^+, as can be seen in Fig. 7(c).

D. Photoluminescence spectra of acceptor-bound exciton

In Figs. 8 and 9, we present the PL spectra of ZnTe and CdTe doped with Cu, Ag, and Cr as well as those nominally pure. Following Venghaus and Dean,[45] the spectral signatures at 2.3750 and 2.3745 eV in Fig. 8 are attributed to excitons bound to Cu and Ag acceptors, respectively. (The corresponding positions in Ref. 45 are 2.3749 and 2.3740 eV, respectively.) The strongest peak in the nominally undoped ZnTe occurs at 2.3745 eV, presumably due to inadvertently introduced Ag acceptors. The strong 2.3753 eV PL feature in Cr-doped ZnTe can be assigned to excitons bound to a Cr acceptor.

For CdTe, the principal acceptor-bound exciton features have been reported[46] at 1.5896 eV for Cu and at 1.5885 eV for Ag. Our PL spectra for Cu- and Ag-doped CdTe, as shown in Fig. 9, reveal the Cu- and Ag-acceptor-bound exciton features at 1.5894 and 1.5888 eV, respectively. The

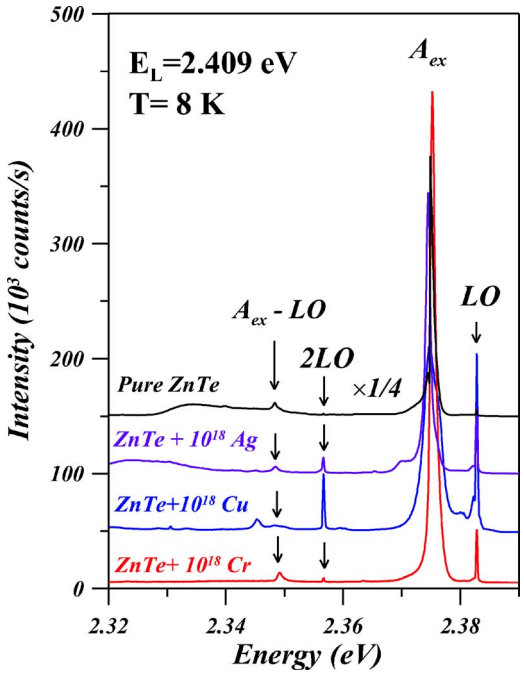

FIG. 8. (Color online) Photoluminescence (PL) spectra of Cu-, Ag-, and Cr-doped ZnTe as well as that of pure ZnTe. The spectra were excited by a 5145 Å line from an Ar^+ laser and recorded at T=8 K. A_{ex} stands for the acceptor-bound exciton and A_{ex}-LO for the combination of A_{ex} with LO.

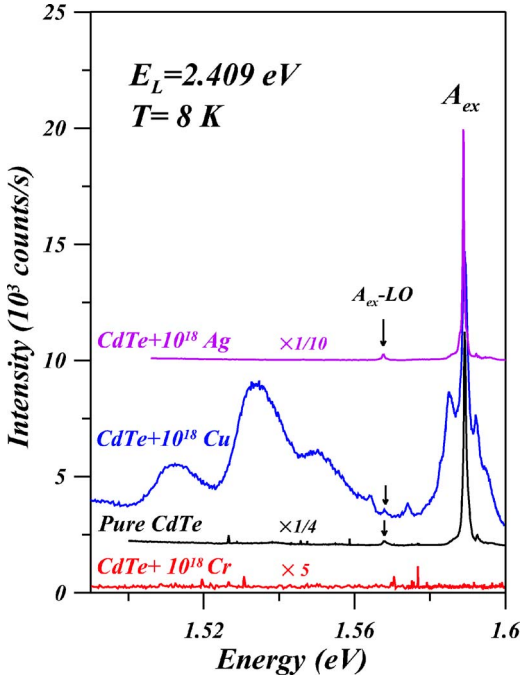

FIG. 9. (Color online) Photoluminescence (PL) spectra of Ag-, Cu-, and Cr-doped CdTe and pure CdTe recorded at $T=8$ K. The spectra were excited by a 5145 Å line from an Ar^+ laser. A_{ex} stands for the acceptor-bound exciton and A_{ex}-LO for the combination of A_{ex} with LO.

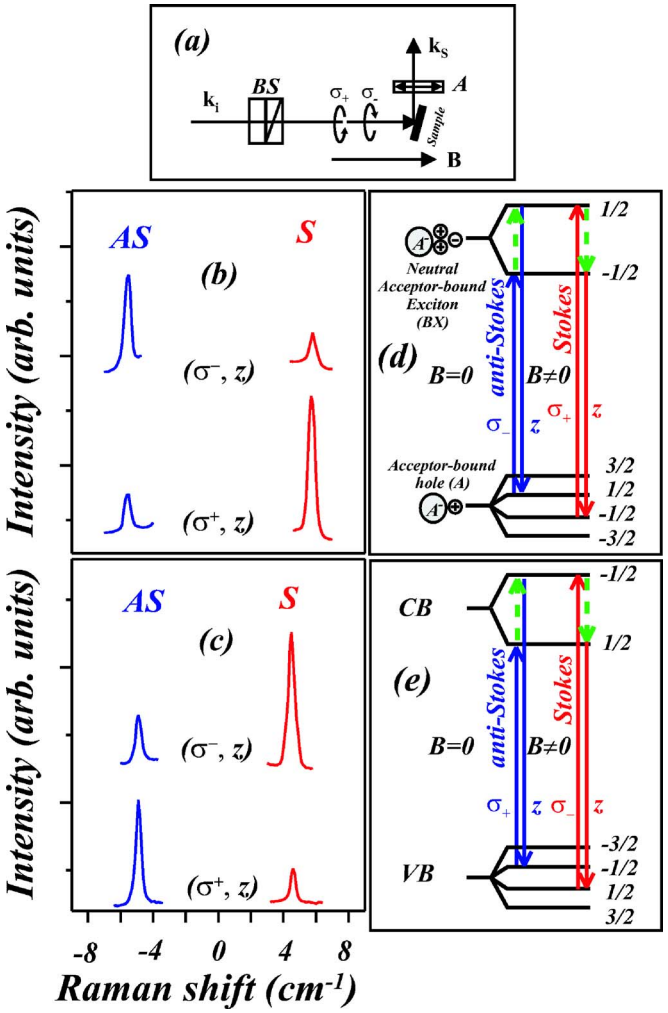

FIG. 10. (Color online) (a) Raman scattering geometry: BS is a Babinet-Soleil compensator and A is a linear analyzer. The comparison of the polarization dependence of the Stokes (S) and anti-Stokes (AS) Raman lines generated by (b) spin-flip Raman transitions between adjacent sublevels of the Zeeman multiplet of Cr^+ in CdTe and (c) spin-flip Raman scattering of donor-bound electrons in pure CdTe. Both the spectra are recorded at 6 K and 6 T, the corresponding Raman mechanisms being (d) for the former and (e) for the latter.

"undoped" pure CdTe, with the principal feature at 1.5893 eV, shows the dominant Cu impurity often present in the starting material. Cr-doped CdTe, however, shows no luminescence features; the absence of the acceptor-bound exciton in PL and the weak free exciton in WMR in Cr-doped CdTe are not fully understood. The near coincidence of the acceptor-bound exciton features for Cu and Ag in ZnTe(CdTe), as comprehensively investigated and intepreted together with the PL of other acceptors (i.e., Li, Na, and Au) in ZnTe and in CdTe by Molva *et al.*,[47] indicates very small central-cell corrections, almost independent of the nature of the acceptor at the cation site. The valence-band parameters, and thus the effective-mass acceptor states in CdTe and ZnTe, are similar. The striking similarity of the acceptor-bound exciton features for Cu-, Ag-, and Cr-doped ZnTe indicates that Cr is also an acceptor.

E. The microscopic mechanism of Raman-EPR of Cr^+ in ZnTe and CdTe

The polarization dependence of the Stokes and anti-Stokes Raman-EPR lines in $Cd_{1-x}Cr_xTe$, in a "pseudo-right-angle" scattering geometry [see Fig. 10(a)], is displayed in Fig. 10(b). With the magnetic field along $\hat{\mathbf{z}}$, $\hat{\sigma}_+=(1/\sqrt{2})(\hat{\mathbf{x}}+i\hat{\mathbf{y}})$ and $\hat{\sigma}_-=(1/\sqrt{2})(\hat{\mathbf{x}}-i\hat{\mathbf{y}})$ are circularly polarized incident radiations of positive and negative helicities, respectively; scattered radiation analyzed along $\hat{\mathbf{z}}$ then yields the $(\hat{\sigma}_+,\hat{\mathbf{z}})$ and $(\hat{\sigma}_-,\hat{\mathbf{z}})$ polarization configurations. In $(\hat{\sigma}_+,\hat{\mathbf{z}})$, the Stokes component is much stronger than the anti-Stokes, whereas the opposite is the case in $(\hat{\sigma}_-,\hat{\mathbf{z}})$. The leakage observed in both configurations can be attributed to the fact that the "pseudo" scattering geometry is not exactly right angle (and hence the label). The exciting radiation $\hbar\omega_L$ needs to be very close to the excitonic transitions for resonance enhancement, on the one hand, but this requirement restricts the scattering to a small volume, on the other; thus the strict exclusion expected in the polarization configuration is not fully realized, but is nevertheless qualitively consistent with the selection rules. The Raman transitions with shifts of $n\hbar\omega_{PM}$ ($n\geqslant 3$) in Figs. 2 and 3 do not satisfy angular momentum conservation in contrast to those with $n=1,2$ and a different mechanism has to be invoked, as discussed in Refs. 48 and 49.

The intensities of the Stokes and anti-Stokes Raman lines as a function of the incident and scattered photon energy, i.e.,

the resonance profiles, are shown in Fig. 11. The Raman-EPR intensity as a function of the incident photon energy, as displayed in Fig. 11(a), shows distinctly different peaks for the Stokes (at 1.5885 eV) and anti-Stokes (1.5869 eV) components, separated by $2\hbar\omega_{PM}$. Adapting Loudon's theory for optical phonons,[50] the differential scattering cross section for the Stokes component, described by a three-step Raman process as schematically illustrated in Fig. 10(d), can be written as

$$\frac{d\sigma}{d\Omega} \propto \left| \frac{\langle n_S+1,0|\hat{H}_{eR}|n_S,b\rangle\langle m_S+1,b|\hat{H}_{ex}|m_S,a\rangle\langle n_I-1,a|\hat{H}_{eR}|n_I,0\rangle}{[\omega_b-(\omega_L-\omega_{PM})][\omega_a-\omega_L]} + \cdots \right|^2, \tag{1}$$

where the ellipsis represents five additional terms. Here, $\hat{H}_{eR}$ is the electron-photon interaction Hamiltonian, $\hat{H}_{ex}$ is the Hamiltonian describing the exchange interaction between magnetic ions and band electrons, n_I and n_S are the occupation numbers of incident and scattered photon modes, and $\hbar\omega_a$, $\hbar\omega_b$ are the intermediate excitation energies of the virtual electron-hole pair. Equivalently, the intensities of the Stokes and anti-Stokes Raman-EPR plotted as a function of the *scattered photon energy* [Fig. 11(b)] show that their maxima coincide; this indicates that the resonance effect arises with the scattered photon energy $\hbar(\omega_L-\omega_{PM})$ equaling $\hbar\omega_b$ in Eq. (1), i.e., it is due to *out resonance*. The zero-field free exciton energy of pure CdTe is 1.5966 eV [see Fig. 1(a)], and the free exciton energy of $Cd_{1-x}Cr_xTe$ can be expected to occur at a still higher energy. On the basis of the ~10 meV difference between the peak energy for the out resonance in the resonance profile (1.5877 eV) and that for the free exciton energy ($\geqslant$1.5966 eV), one can rule out the possibility that the Raman-EPR in Figs. 3 and 5 is mediated by a free exciton. In contrast, the energies of an acceptor-bound exciton, as shown in Fig. 9 (1.5888 eV for an Ag acceptor and 1.5894 eV for a Cu acceptor), are close to the peak energy of out resonance. It is thus reasonable to attribute the microscopic process of the Raman-EPR of Cr^+ in CdTe as mediated via an exciton bound to a neutral acceptor (Cr, Ag, and/or Cu), analogous to the role played by an exciton bound to a neutral donor[39] in spin-flip Raman scattering from donor-bound electrons in pure CdTe.

The initial and final states of the Raman process mediated by an exciton bound to a neutral acceptor in a magnetic field as depicted in Fig. 10(d) are the Zeeman components of the ground state of the neutral acceptor (A). The intermediate state is one of the Zeeman levels derived from the ground state of an exciton bound (BX) to the neutral acceptor. The Zeeman components of the ground state of a neutral acceptor (A), i.e., an acceptor-bound hole, are those of a hole. The Zeeman levels of an exciton bound (BX) to a neutral acceptor are those of an electron, since the spins of the two holes are antiparallel. The reasons for the ordering of the Zeeman sublevels of an electron and a hole in $Cd_{1-x}Cr_xTe$ are explained in the next paragraph. Thus, the excitonic Zeeman level scheme of an exciton bound to a neutral acceptor is similar to that of a free exciton. The Stokes process of the Raman-EPR can be described as follows:[48] (i) in the first step, an incident photon of polarization $\hat{\sigma}_+$ excites an electron from $|-1/2\rangle_A$ to $|1/2\rangle_{BX}$; (ii) in the intermediate step, the electron interacts with a Cr^+ ion, through a simultaneous spin flip of the electron with $\Delta M_s(e)=-1$, that of the Cr^+ ion with $\Delta M_s(Cr^+)=1$; (iii) and in the final step, the electron deexcites from $|-1/2\rangle_{BX}$ to the initial $|-1/2\rangle_A$ by emitting a photon of polarization $\hat{\mathbf{z}}$ yielding a net photon energy $\hbar\omega_S=\hbar\omega_L-\hbar\omega_{PM}$. In the Stokes process, the Cr^+ ion experiences $\Delta M_s(Cr^+)=1$ transitions between its Zeeman sublevels. Similarly, the anti-Stokes process corresponds to the deexcitation of Cr^+ to the next lower Zeeman sublevel with $\Delta M_s(Cr^+)=-1$.

It is interesting to note that, unlike the electron spin-flip transitions between Zeeman multiplets of Cr^+, the spin-flip

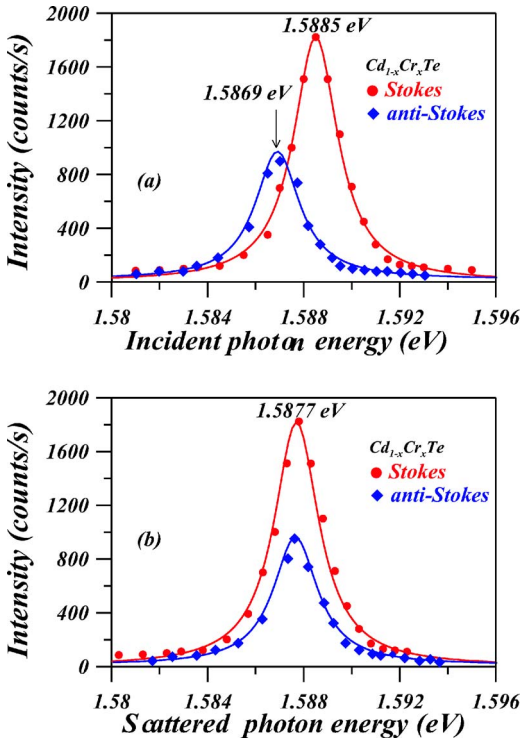

FIG. 11. (Color online) Resonance profiles of Stokes and anti-Stokes Raman lines for the Raman-EPR of Cr^+ in CdTe as a function of (a) incident photon energy and (b) scattered photon energy. The circles and squares are experimental data. The solid curves are Lorentzian fits to the data. All the data are recorded at 8 K and 6 T.

Raman scattering (SFRS) of donor-bound electrons in pure CdTe, as shown in Fig. 10(c), exhibits opposite polarization selection rules. For comparison, the Raman process for SFRS of donor-bound electrons mediated by a free exciton[39] is shown in Fig. 10(e). The difference between Fig. 10(d) and Fig. 10(e) is the ordering of sublevels of the electron, as well as those of the hole (or valence-band electron). In pure CdTe, the Zeeman sublevels are ordered, as shown in Fig. 10(e). However, in Fig. 10(d) for $Cd_{1-x}Cr_xTe$, the ferromagnetic *s-d* exchange interaction dominates, reversing the sequence of the $|1/2\rangle$ and $|-1/2\rangle$ levels; similarly, the ferromagnetic *p-d* exchange interaction in Cr-based DMSs also reverses the ordering of the valence-band Zeeman sublevels,[5] in comparison to that in Mn-, Fe-, and Co-based DMSs,[40,48] which show an antiferromagnetic *p-d* exchange interaction.

IV. CONCLUDING REMARKS

The isotropic *g* factor of the Raman-EPR close to 2, characteristic of Cr^+, not of Cr^{2+} and Cr^{3+}; the photoconversion of Cr^{2+} into Cr^+; the close similarity in PL spectra of the excitons bound to Cr^+ centers with those of Ag and Cu acceptors in ZnTe; etc., these experimental results emerging from the present investigation constitute a convincing case for the existence of Cr^+ as an acceptor in both ZnTe and CdTe, originating in the $3d^5$ electronic configuration of the *d* shell of Cr^+. Taken together with magnetization, it is clear that Cr^+ is a minority electronic configuration, in contrast to Cr^{2+} which is dominant. Nevertheless, the Cr^+ state has been selectively observed in EPR and Raman-EPR.

The synthesis of $Cd_{1-x}Cr_xTe$ and $Zn_{1-x}Cr_xTe$ employing the nonequilibrium growth techniques such as MBE or MOCVD may produce specimens with *x* significantly larger than those available to date. It would be of particular interest to investigate the *sp-d* exchange interaction using magnetoreflectivity for such high Cr-based DMSs for a direct observation of the striking ferromagnetic *p-d* exchange interaction. With the introduction of donors, e.g., Ga or Cl, in these DMSs, the exploration of the spin-flip Raman scattering (SFRS) from donor-bound electrons would be another interesting problem worthy of study. Twardowski *et al.* have reported[51] the observation of SFRS from donor-bound electrons in $Cd_{1-x}Cr_xS$, while Herbich *et al.*[52] have explored theoretically the nature of the magnetic polaron in Cr-based DMSs. We also note here that we have observed SFRS from donor-bound electrons in $Cd_{1-x}Cr_xSe$.[53]

ACKNOWLEDGMENTS

The authors thank the National Science Foundation for its support through Grant No. DMR-0405082 and Purdue University for its support through the Academic Reinvestment Program.

[1] *Semiconductors and Semimetals*, edited by J. K Furdyna and J. Kossut (Academic, San Diego, 1988), Vol. 25.
[2] J. Blinowski, P. Kacman, and H. Przybylińska, Solid State Commun. **79**, 1021 (1991); J. Blinowski and P. Kacman, Phys. Rev. B **46**, 12298 (1992); J. Blinowski, P. Kacman, and J. A. Majewski, J. Cryst. Growth **159**, 972 (1996).
[3] A. K. Bhattacharjee, Phys. Rev. B **46**, 5266 (1992); **49**, 13987 (1994).
[4] W. Mac, Nguyen The Khoi, A. Twardowski, J. A. Gaj, and M. Demianiuk, Phys. Rev. Lett. **71**, 2327 (1993).
[5] W. Mac, A. Twardowski, and M. Demianiuk, Phys. Rev. B **54**, 5528 (1996).
[6] W. Mac, Nguyen The Khoi, A. Twardowski, and M. Demianiuk, J. Cryst. Growth **159**, 993 (1996).
[7] M. Herbich, W. Mac, A. Twardowski, K. Ando, Y. Shapira, and M. Demianiuk, Phys. Rev. B **58**, 1912 (1998).
[8] H. Saito, V. Zayets, S. Yamagata, and K. Ando, Phys. Rev. Lett. **90**, 207202 (2003).
[9] H. Saito, V. Zayets, S. Yamagata, and K. Ando, J. Appl. Phys. **93**, 6796 (2003).
[10] S. A. Wolf, D. D. Awschalom, R. A. Buhrman, J. M. Daughton, S. von Molnár, M. L. Roukes, A. Y. Chtchelkanova, and D. M. Treger, Science **294**, 1488 (2001).
[11] T. M. Pekarek, D. J. Arenas, B. C. Crooker, I. Miotkowski, and A. K. Ramdas, J. Appl. Phys. **95**, 7178 (2004).
[12] J. T. Vallin and G. D. Watkins, Phys. Rev. B **9**, 2051 (1974).
[13] M. E. J. Boonman, W. Mac, A. Twardowski, A. Wittlin, P. J. M van Bentum, J. C. Maan, and M. Demianiuk, Phys. Rev. B **61**, 5358 (2000).
[14] J. T. Vallin, G. A. Slack, S. Roberts, and A. E. Hughes, Phys. Rev. B **2**, 4313 (1970).
[15] A. Twardowski, P. Glód, W. J. M. de Jonge, and M. Demianiuk, Solid State Commun. **64**, 63 (1987).
[16] W. Mac, A. Twardowski, P. J. T. Eggenkamp, H. J. M. Swagten, Y. Shapira, and M. Demianiuk, Phys. Rev. B **50**, 14144 (1994).
[17] T. M. Pekarek, J. E. Luning, I. Miotkowski, and B. C. Crooker, Phys. Rev. B **50**, 16914 (1994).
[18] T. M. Pekarek, I. Miotkowski, and B. C. Crooker, J. Appl. Phys. **79**, 6436 (1996).
[19] J. Dieleman, R. S. Title, and W. V. Smith, Phys. Lett. **1**, 334 (1962).
[20] P. H. Kasai and Y. Otomo, Phys. Rev. Lett. **7**, 17 (1961).
[21] R. S. Title, Phys. Rev. **131**, 623 (1963).
[22] H. D. Fair, R. D. Ewing, and F. E. Williams, Phys. Rev. **144**, 298 (1966).
[23] T. Buch, B. Clerjaud, and B. Lambert, Phys. Rev. B **7**, 184 (1973).
[24] M. Godlewski and M. Kamińska, J. Phys. C **13**, 6537 (1980).
[25] R. S. Title, Phys. Rev. **133**, A1613 (1964).
[26] T. L. Estle and W. C. Holton, Phys. Rev. **150**, 159 (1966).
[27] G. W. Ludwig and M. R. Lorenz, Phys. Rev. **131**, 601 (1963).
[28] R. Rai, J. Y. Savard, and B. Tousignant, Phys. Lett. **25A**, 443 (1967).
[29] C. Parks, Ph.D. thesis, Purdue University, 1994.
[30] M. J. Seong, H. Alawadhi, I. Miotkowski, A. K. Ramdas, and S. Miotkowska, Solid State Commun. **112**, 329 (1999).

[31] Chee-Leung Mak, R. Sooryakumar, B. T. Jonker, and G. A. Prinz, Phys. Rev. B **45**, 3344 (1992).
[32] M. Villeret, S. Rodriguez, and E. Kartheuser, Phys. Rev. B **41**, 10028 (1990).
[33] D. Colignon, E. Kartheuser, S. Rodriguez, and M. Villeret, J. Cryst. Growth **159**, 875 (1996).
[34] J. Lambe and C. Kikuchi, Phys. Rev. **119**, 1256 (1960).
[35] A. Abragam and B. Bleaney, *Electron Paramagnetic Resonance of Transition Ions* (Clarendon, Oxford, 1970).
[36] P. Christmann, J. Kreissl, D. M. Hofmann, B. K. Meyer, R. Schwarz, and K. W. Benz, J. Cryst. Growth **161**, 259 (1996).
[37] J. Kreissl, K. Irmscher, P. Peka, M. U. Lehr, H.-J. Schulz, and U. W. Pohl, Phys. Rev. B **53**, 1917 (1996).
[38] A. Oshiyama, N. Hamada, and H. Katayama-Yoshida, Phys. Rev. B **37**, 1395 (1988).
[39] S. Tsoi, I. Miotkowski, S. Rodriguez, A. K. Ramdas, H. Alawadhi, and T. M. Pekarek, Phys. Rev. B **69**, 035209 (2004).
[40] A. Petrou, D. L. Peterson, S. Venugopalan, R. R. Galazka, A. K. Ramdas, and S. Rodriguez, Phys. Rev. B **27**, 3471 (1983).
[41] A. Petrou, D. L. Peterson, S. Venugopalan, R. R. Galazka, A. K. Ramdas, and S. Rodriguez, Phys. Rev. Lett. **48**, 1036 (1982).
[42] P. Y. Yu and M. Cardona, *Fundamentals of Semiconductors* (Springer, New York, 1996), p. 368.
[43] R. Loudon, Proc. R. Soc. London, Ser. A **275**, 218 (1963); for a review, see M. Cardona, *Light Scattering in Solids II*, edited by M. Cardona and G. Güntherodt (Springer, Berlin, 1982), pp. 19–178.
[44] W. Limmer, S. Bauer, H. Leiderer, W. Gebhardt, A. Cantarero, C. Trallero-Giner, and M. Cardona, Phys. Rev. B **45**, 11709 (1992).
[45] H. Venghaus and P. J. Dean, Phys. Rev. B **21**, 1596 (1980).
[46] J. P. Chamonal, E. Molva, and J. L. Pautrat, Solid State Commun. **43**, 801 (1982).
[47] E. Molva, J. L. Pautrat, K. Saminadayar, G. Milchberg, and N. Magnea, Phys. Rev. B **30**, 3344 (1984).
[48] M. J. Seong, H. Alawadhi, I. Miotkowski, A. K. Ramdas, and S. Miotkowska, Phys. Rev. B **63**, 125208 (2001).
[49] D. L. Peterson, D. U. Bartholomew, A. K. Ramdas, and S. Rodriguez, Phys. Rev. B **31**, 7932 (1985); R. G. Alonso, E.-K. Suh, A. K. Ramdas, N. Samarth, H. Luo, and J. K. Furdyna, *ibid.* **40**, 3720 (1989). J. Stúhler, G. Schaack, M. Dahl, A. Waag, G. Landwehr, K. V. Kavokin, and I. A. Merkulov, Phys. Rev. Lett. **74**, 2567 (1995).
[50] R. Loudon, Adv. Phys. **13**, 423 (1964).
[51] A. Twardowski, D. Heiman, M. T. Liu, Y. Shapira, and M. Demianiuk, Phys. Rev. B **53**, 10728 (1996).
[52] M. Herbich, A. Twardowski, D. Scalbert, and A. Petrou, Phys. Rev. B **58**, 7024 (1998).
[53] X. Lu, I. Miotkowski, S. Rodriguez, A. K. Ramdas, H. Alawadhi, and T. M. Pekarek (unpublished).
[54] The LO phonon in $Zn_{1-x}Cr_xTe$ and $Cd_{1-x}Cr_xTe$, with Raman shift at 210 and 171 cm^{-1}, respectively, is essentially that of pure ZnTe and CdTe. Due to the low Cr concentration, no CrTe-related phonon modes are observed in our investigations.